VI International Conference on Computational Methods for Coupled Problems in Science and Engineering
COUPLED PROBLEMS 2015
B. Schrefler, E. Oñate and M. Papadrakakis(Eds)

FINITE STRAINS FULLY COUPLED ANALYSIS OF A HORIZONTAL WELLBORE DRILLED THROUGH A POROUS ROCK FORMATION

N. Spiezia[†*], **V. Salomoni**[†] **C. Majorana**[†]

[†]Department of Civil, Environmental and Architectural Engineering (DICEA)
University of Padua
Via Marzolo 9, 35131 Padova, Italy
e-mail: nicolo.spiezia@dicea.unipd.it

Key words: Wellbore instability, solid-displacement/fluid-diffusion problem, finite strain elastoplasticity.

Abstract. Wellbore instability, in particular in deep perforations, continues to be one of the major problem in the oil and gas industry, that can dramatically increase production costs. Eventual instabilities may be prevented supporting temporarily the wellbore with mud circulation. If instability may occur, the value of the mud pressure needs to be sufficiently high to prevent compressional failure, but it should also be lower than a critical value that would cause tensile failure and unintentional hydraulic fracturing. Predicting faithfully the stress distribution around a borehole, and moreover the yielding and failure zones, is a challenging but fundamental task, essential to estimate the correct mud pressure and hence to prevent instabilities and sand production. This study focuses on quantifying the pressure distribution, stress field and plastic zones around a horizontal borehole drilled at great depth through a highly porous rock formation. The perforation of a wellbore in a saturated porous material is a coupled problem, which involves deformations of the solid phase and simultaneous diffusion of the fluid phase. A fully coupled finite element method is adopted, considering both material non linearity (elastoplasticity) and geometric nonlinearity (finite deformations) in the solid matrix, resulting in a so called $\boldsymbol{u}-p$ formulation. The variation of porosity and permeability, as consequence of the finite deformations of the solid matrix, is taken into account. The model adopts an elastoplastic constitutive law characterized by two yield surfaces, that is able to capture the dilatant and compactant plastic mechanism. The simulations investigate the quasi-static transient phenomenon associated with the perforation, until the steady state condition is reached. The model describes the evolution of the stress and pressure distribution, and moreover the propagation of the plastic zones around the borehole. The work demonstrates the capability of the finite deformations coupled approach to simulate the whole process, giving an instrument to determine the stability and sand production of the wellbore.

1 INTRODUCTION

Wellbore instability is still one of the major problem in the oil and gas industry, with disruptive consequence in the perforation and exploitation costs [1]. The instability of a wellbore is the effect of the failure of the rock surrounding the borehole, which may collapse under the new stress distribution due to the perforation.

In order to prevent instabilities during the drilling process, the wellbore is temporarily supported by the mud pressure [2]. The value of the mud pressure has to be properly determined: if the value is too low, compressional failure may occur around the wall of the hole. On the other hand, if the value of the mud pressure is too high, tensile failure may occur, causing unintentional hydraulic fracturing. Even if the risk of complete failure is avoided, the limitation of the failure zones is desirable, to reduce as much as possible the production of sand. For all these reasons, predicting faithfully the stress distribution around a borehole - and moreover the yielding and failure zones - is a fundamental task, essential to decide the most appropriate range of values for the mud pressure.

Traditionally, the stability of a well is determined using models based on linear elasticity, where failure is assumed to occur when the stress along the wall of the hole reaches the failure strength of the rock. An improvement in the assessment of the stability is given by numerical simulations, in particular with Finite Element Models. FEM analysis, endowed with elastoplastic constitutive law, can provide a more realistic evaluation of stability, with the advantage of being able to delineate the extent of the damaged region [3, 4, 5]. However, the complete drilling process can be properly simulated only if the interaction between the fluid phase and the solid phase is taken into account. Normally, these two fields are treated as separate issues and the tendency for each field is to simplify and make approximate assumptions for the other field. This is expected because of the complexity of treating geomechanics and multiphase fluid flow as coupled processes.

The aim of this study is to quantify the pressure and stress distribution and the propagation of plastic zones around a horizontal borehole drilled at great depth through a highly porous rock formation. The solid-displacements/fluid-diffusion problem is simulated with a fully coupled finite element method, resulting in a so called $\boldsymbol{u}-p$ formulation [7]. The model assumes finite strains formulation, which guarantees the correctness of the method, even in case of large deformation of the solid matrix. The variation of porosity and permeability, as consequence of the finite deformations of the solid matrix, is taken into account. The constitutive behavior of the porous rock formation is described by an elastoplastic cap model. In fact, highly porous rock are susceptible to different failure mechanisms, mainly due to shear-induced dilation and shear-enhanced compaction. Hence, the model is characterized by two yield surfaces, in order to capture the dilatant plastic mechanism and the compactant plastic mechanism.

The paper is organized as follow: section two briefly recall the finite strains coupled formulation for a fully saturated porous media. Section three deals with the constitutive laws adopted for the solid phase and the fluid phases. Section four presents the numerical

results of a wellbore considered ad example, drilled in an high porous rock formation, to illustrate the importance of coupling rock deformation and fluid flow. Finally, section five draws the conclusion of the presented work and gives an insight of the future developments of the research.

2 THEORETICAL FRAMEWORK

In this section we briefly recall the balance laws that govern the solid-displacement/fluid-diffusion problem in the fully saturated porous rock formation [7]. The fundamental idea consists in writing the mass balance and linear momentum equations for a two phase continuum body. We use mixture theory to formulate the kinematics of deformation of the solid matrix containing the fluid within its pores. We denote the motion of the solid matrix by $\varphi_s(\boldsymbol{X}_s, t)$ where $\boldsymbol{X}_s = \boldsymbol{X}$ is the position vector of the solid material point X in the reference configuration, the motion of fluid by $\varphi_f(\boldsymbol{X}_f, t)$, where $\boldsymbol{X}_f$ is the initial position vectors of fluid. Referring to the motion of the solid, we can write the material time derivatives following the fluid motion in terms of the material time derivative following the solid motion as

$$\frac{\mathrm{d}^f(\cdot)}{\mathrm{d}t} = \frac{\mathrm{d}(\cdot)}{\mathrm{d}t} + \nabla^{\boldsymbol{x}}(\cdot) \cdot \tilde{\boldsymbol{v}}, \tag{1}$$

where $\tilde{\boldsymbol{v}} := \boldsymbol{v}_f - \boldsymbol{v}$ is the velocity of the fluid with respect to the solid.
Let $\boldsymbol{x} = \varphi(\boldsymbol{X}, t)$ denote the position of the solid material point X and $\boldsymbol{F} = \partial \boldsymbol{x}/\partial \boldsymbol{X}$ the associated deformation gradient of the solid matrix, with the Jacobian J such that $J = \det(\boldsymbol{F}) = \mathrm{d}v/\mathrm{d}V$. We denote the volume fraction ϕ^α of the constituent α as the ratio between its volume $\mathrm{d}V^\alpha$ divided by the total volume of the mixture $\mathrm{d}V$, that is, $\phi^\alpha = \mathrm{d}V^\alpha/\mathrm{d}V$. Therefore,

$$\phi^s + \phi^f = 1 \tag{2}$$

The partial mass density of constituent α is given by $\rho^\alpha = \phi^\alpha \rho_\alpha$, where ρ_α is the intrinsic mass density of constituent α. This gives

$$\rho^s + \rho^f = \rho \tag{3}$$

where ρ is the total mass density of the mixture.
With these preliminaries, the conservation of mass equation for the solid and fluid phases are respectively

$$\dot{\rho}^s + \rho^s \nabla^{\boldsymbol{x}} \cdot \boldsymbol{v} = 0; \tag{4}$$

$$\dot{\rho}^f + \rho^f \nabla^{\boldsymbol{x}} \cdot \boldsymbol{v} = -\boldsymbol{\nabla}^{\boldsymbol{x}} \cdot \boldsymbol{q}, \tag{5}$$

where $\boldsymbol{q} \equiv \rho^f \tilde{\boldsymbol{v}}$ is the Eulerian relative flow vector of the fluid phase with respect to the solid matrix. Adding Eqs. (4) and (5), we get the basic conservation of mass equation for the system, i.e.

$$\dot{\rho}_0 = -J \nabla^{\boldsymbol{x}} \cdot \boldsymbol{q}, \tag{6}$$

where $\rho_0 \equiv J\rho$ is the pull-back mass density of the mixture in the reference configuration. In order to formulate the balance of linear momentum, a thermodynamically consistent effective stress equation may be written in terms of the total Cauchy stress tensor $\boldsymbol{\sigma}$, effective Cauchy stress tensor $\boldsymbol{\sigma}'$ and pore fluid pressure p as

$$\boldsymbol{\sigma} = \boldsymbol{\sigma}' - Bp\mathbf{1}, \tag{7}$$

where $B = 1 - K/K_s$ is the Biot coefficient and K is the bulk modulus of the solid matrix. To impose the balance of linear momentum with respect to the undeformed configuration, we need to introduce the first Piola-Kirchhoff stress tensor $\boldsymbol{P}$, which holds

$$\boldsymbol{P} = \boldsymbol{\tau} \cdot \boldsymbol{F}^{-T} = \boldsymbol{\tau}' \cdot \boldsymbol{F}^{-T} - B\theta_f \boldsymbol{F}^{-T} \tag{8}$$

where $\boldsymbol{\tau} = J\boldsymbol{\sigma}$ is the symmetric total Kirchhoff stress tensor, $\boldsymbol{\tau}' = J\boldsymbol{\sigma}'$ is the effective Kirchhoff stress tensor and $\theta_f = Jp$ is the Kirchhoff pore fluid pressure. Ignoring inertia forces, the balance of linear momentum in Lagrangian form can be written as

$$\nabla^{\boldsymbol{X}}(\boldsymbol{P}) + \rho_0 \boldsymbol{g} = \mathbf{0}. \tag{9}$$

The balance laws (6) and (9), in addition with the constitutive laws developed in the next section, provide a complete set of governing equations, which allow for the solution of quasi-static deformation-diffusion boundary-value problems. After developing the variational form, the problem results in a parabolic system where the displacements of the solid phase and the pore pressures are the basic unknowns in an updated Lagrangian finite element scheme.

3 CONSTITUTIVE MODELS

For the solid phase, we employ an elastoplastic model based on the multiplicative decomposition of deformation gradient and product formula algorithm described by Simo [9]. The elastic region is assumed to be governed by an isotropic strain-energy function as follow

$$\Psi = \frac{1}{2}\lambda[\epsilon_1^e + \epsilon_2^e + \epsilon_3^e]^2 + \mu[(\epsilon_1^e)^2 + (\epsilon_2^e)^2 + (\epsilon_3^e)^2], \tag{10}$$

where λ and μ are the classical Lamé constants and $\varepsilon_a^e = \ln \lambda_a^e$, with λ_a^e $(a = 1, 2, 3)$ the principal elastic stretches. The Kirchhoff effective stress tensor $\boldsymbol{\tau}'$ is coaxial with the left elastic Cauchy-Green deformation tensor $\boldsymbol{b}^e = \boldsymbol{F}^e \cdot \boldsymbol{F}^{eT}$ and defined such that

$$\boldsymbol{\tau}' = 2\frac{\partial \Psi}{\partial \boldsymbol{b}^e} \cdot \boldsymbol{b}^e. \tag{11}$$

The plastic region is defined in terms of stress invariants of the effective Kirchhoff stress tensor

$$P = \frac{1}{3}\mathrm{tr}(\boldsymbol{\tau}') \qquad Q = \sqrt{\frac{3}{2}}\,\|\boldsymbol{s}\|\,, \tag{12}$$

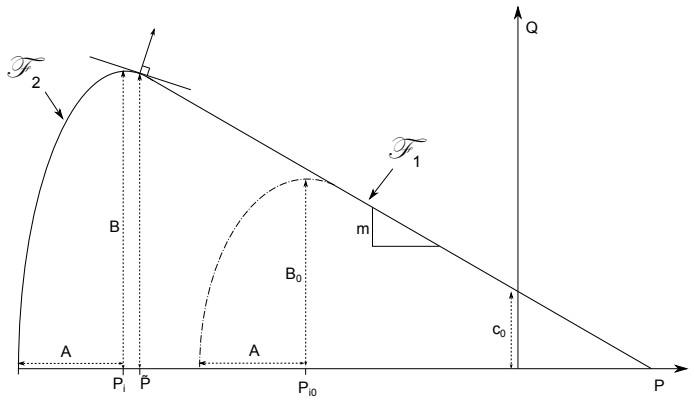

Figure 1: Schematic representation of the elastoplastic constitutive model for the high porous rock.

where $\boldsymbol{s} = \boldsymbol{\tau}' - P\mathbf{1}$. The yield function is characterized by two surfaces $\mathscr{F}_1$ and $\mathscr{F}_2$, that intersect smoothly: a linear surface to capture the dilatant shear failure and an elliptical surface to capture the compactant mechanical behavior of high porous rock. The yield functions, in the Kirchhoff stress invariants space, take the form

$$\mathscr{F}_1(P,Q) = Q - mP - c_0 = 0 \qquad \mathscr{F}_2(P,Q,P_i) = B^2(P-P_i)^2 + A^2Q^2 - A^2B^2 = 0 \tag{13}$$

where m is the slope of the linear yield surface, associated with the frictional angle, c_0 is the cohesion, A and B are respectively the minor and major semi-axis of the ellipse and P_i is the centroid. The intersection between the two surfaces is defined as the point in which $\mathscr{F}_1$ is tangent to $\mathscr{F}_2$, ensuring that the two surfaces produce a unique surface without any angular point. Hardening is admissible only along the compactant side, since the elliptical surface contracts and expands depending on the accumulated plastic volumetric strain ϵ_v^p, maintaining a constant width (i.e. $A = A_0$) [10] and remaining always tangent to the linear surface, as follow

$$P_i = P_{i_0}\left(\frac{\epsilon^*}{\epsilon^* - \epsilon_v^p}\right)^r \tag{14}$$

where P_{i_0} is the initial value, ϵ^* is the volumetric deformation at ultimate compaction and r is the exponent that control the rate of volumetric hardening [11]. A non associative flow rule is assumed only for the linear side, with a plastic potential of the form

$$\bar{\mathscr{G}} = Q - \bar{m}P - \bar{c} = 0. \tag{15}$$

This non-associative law, assuming that $\bar{m} < m$, avoid the often excessive dilatancy predicted by the associative rule. Fig. 1 summarizes all the relevant information of the elastoplastic model.

The constitutive relation for the fluid phase is given by the generalized Darcy's law, which takes the form

$$\phi^f \tilde{\boldsymbol{v}}_{\boldsymbol{f}} = -\boldsymbol{k} \cdot \boldsymbol{\nabla} \left(\frac{\theta_f}{\rho_f g} + z \right), \tag{16}$$

where g is the gravity acceleration constant and z is the elevation potential. We consider the following evolution of the hydraulic conductivity isotropic tensor, to express the change of permeability with deformation through the Jacobian J with the Kozeny-Carman equation

$$\boldsymbol{k} = k_s(J) = \frac{g\rho_f}{\mu} \frac{D^2}{180} \frac{(J - \phi_0^s)^3}{J(\phi_0^s)^2} \mathbf{1}, \tag{17}$$

with μ is the dynamic viscosity of the fluid, D is the diameter of the grains, and $\phi_0^s = 1 - \phi_0^f$.

4 NUMERICAL SIMULATIONS

The balance equations and the constitutive laws proposed have been implemented in a non linear finite element code, following standard procedures. To show the capability of the method, we investigate a horizontal wellbore drilled in Campos Basin field [12], a reservoir located 290 Km offshore Brazil cost. The parameters of numerical simulations are as follow: $E = 3500$ MPa, $\nu = 0.15$, $\phi_0^f = 0.3$, $m = -1.08$, $c_0 = 10$ MPa, $\bar{m} = -0.15$, $\mu = 0.1$ Kg/ms, $D = 0.01$ mm, $B = 0.6$. As far as the in-situ geostatic stresses in the reservoir production region, the total horizontal stresses are equal in both principal directions, and read $S_H = S_h = 41.4$ MPa. The total vertical stress is assumed to be $S_V = 64.5$ MPa. The pore fluid pressure in the reservoir is equal to $P_p = 32$ Mpa. The open-hole wellbore radius is $R = 107.95$ mm. The wellbore axis is parallel to the direction of the principal horizontal far-field stress S_h. Numerical analysis assumes a plane strain condition. Hence, the principal stress acting on the plane of the borehole section are the vertical and the horizontal stress.

The domain is discretized with quadrilateral elements, endowed with 9 nodes for displacements unknowns and 4 nodes for pressure unknowns, integrated over 9 Gauss point. The finite element geometry, with the boundary conditions, is represented in Fig. 2.

The analysis consists in two phases: in the first phase, the in-situ stresses and the reservoir pore pressure are applied to the complete domain - i.e. as the rock formation is still intact - in order to simulate the in-situ condition before the drilling process. In the second phase, in order to simulate the drilling process, the elements corresponding to the borehole are progressively removed from the domain, decreasing the stiffness and increasing the permeability. At the same time, the value of the mud pressure is applied to the nodes along the wall. This process is simulated instantaneously, assuming just for computational reason a period of time of 0.02 s.

The Fig. 3 represents the results in term of pore pressure (top row) and vertical displacements (bottom row) in case of balanced drilling ($\Delta P = 0$ MPa), i.e when the mud pressure equals the reservoir pore pressure. When the rock is drilled, the pressure distri-

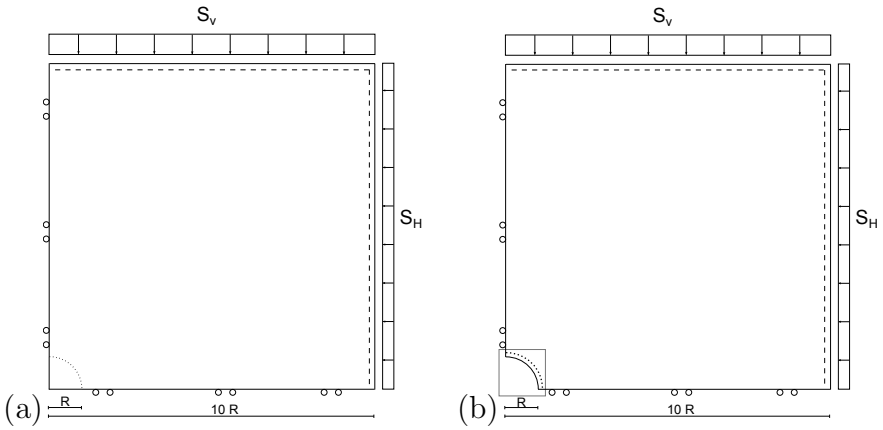

Figure 2: Plane strain domain of a quarter of the borehole. (a) In-situ configuration (no hole): far field stress and reservoir pressure applied (dashed line). (b) Drilling configuration (with hole): far field stress, reservoir pressure (dashed line) and mud pressure (dotted line) applied, with the hole. The box is zoomed in Fig. 5

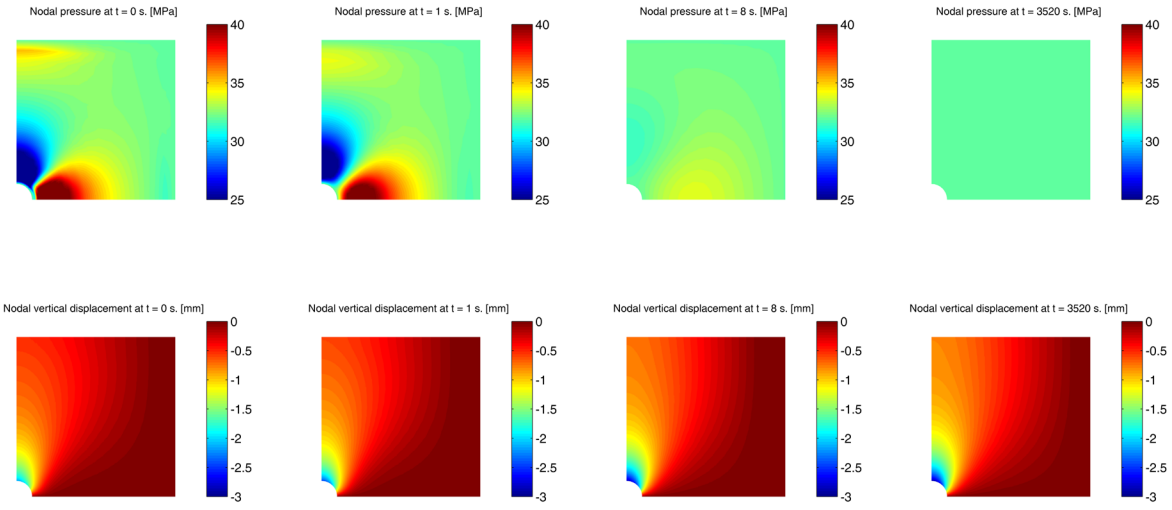

Figure 3: Wellbore drilling simulation with $\Delta P = 0$ MPa. Top images: nodal pore pressure distribution over time. Bottom images: vertical displacements over time.

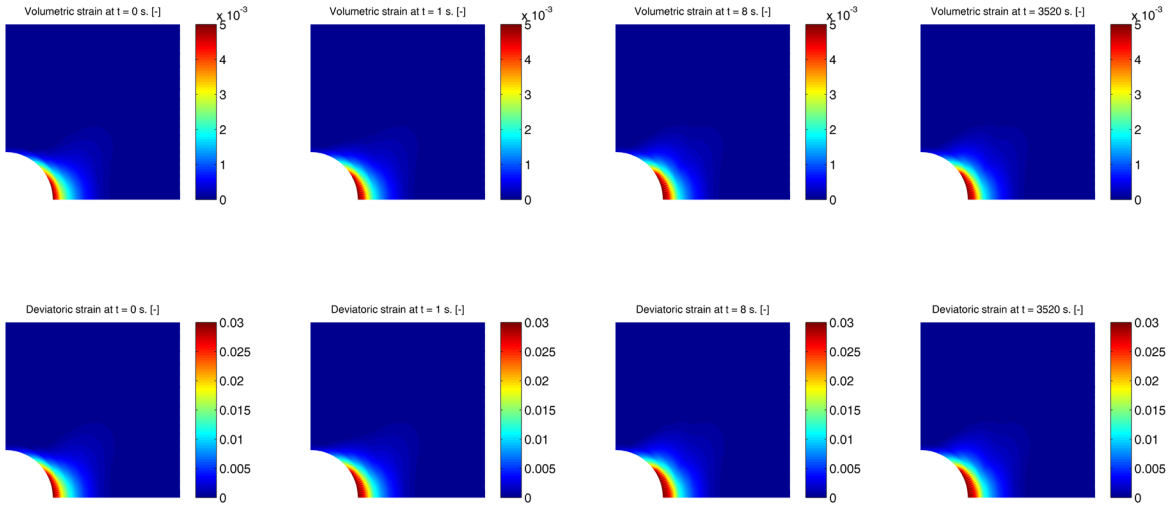

Figure 4: Wellbore drilling simulation with $\Delta P = 0$ MPa. Top images: Plastic volumetric strains over time. Bottom images: Plastic deviatoric strains over time.

bution immediately change significantly. An increment of pressure along the direction of the minimum stress is observed, associated with a decrease of pressure along the direction of maximum stress. This is due to the fact that initially the new load configuration in the rock formation is transferred only to the fluid. Then, the fluid diffuses through the rock until the considered domain reaches an uniform pressure distribution. The diffusion process is associated with the increase of vertical displacements (Fig. 3, bottom row), in close analogy with a consolidation process. The displacements are concentrated along the direction of the maximum stress, increasing in the area along the wall of the hole.
The Fig. 4 represents the results in terms of volumetric (top row) and deviatoric (bottom row) plastic strain. The fluid diffusion determines the expansion of the plastic zone along the wall of the wellbore, as consequence of the increase of the effective stress. The plastic zone is located along the direction of the minimum in-situ stress and involve a significant portion of the rock along the hole. This plastic zone is associated exclusively with the dilatant plastic mechanism (demonstrated by the positiveness of the volumetric plastic strain ϵ_v^p), which means that, for the considered stress configuration, the rock is not subjected to a compactant plastic mechanism.

Following results show the effect of the mud pressure on the drilling process. Two additional configurations are considered, namely with the mud pressure equal to $P_m = 30$ MPa (under-balanced drilling with $\Delta P = 2$ MPa) and the mud pressure equal to $P_m = 36$ MPa (over-balanced drilling with $\Delta P = 4$ MPa). The vertical displacement of point A (see Fig. 5) over time is represented in Fig. 6 in the three different configurations. The severe increase of displacements (about 2 mm) in the first instants is associated with

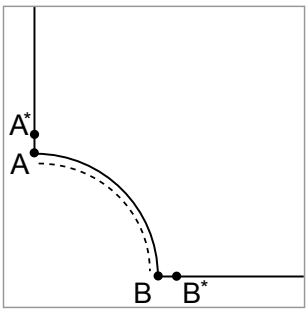

Figure 5: Detail of the domain around the hole. The point with star is located 18 mm far from the hole.

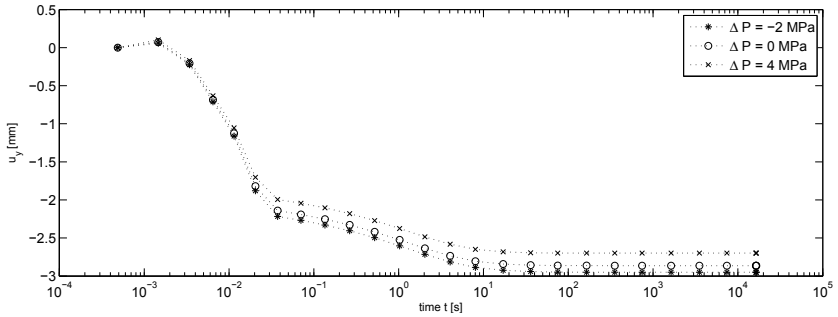

Figure 6: Vertical displacement of point A with different value of mud pressure.

the drilling phase (simulated instantaneously, assuming just for computational reason a period of time of 0.02 s). Then, there is a progressive increase of the vertical displacement due to the diffusion process of the fluid (about 1 mm). The incrementation of the mud pressure, as expected, reduces the vertical displacements, thanks to the contrast furnished to the settlements.

The Fig. 7 represents the evolution of the pore pressure in the point A* (i.e. along the direction of the maximum stress), for the three different values of mud pressure. As can be observed, there is an initial drop of the pressure, associated with the drilling process, until the pore pressure reaches the lowest value. Subsequently, the pore pressure increase progressively, due to the diffusion of the fluid, until the steady state condition, which depends on the mud pressure applied (respectively 30, 32 and 36 MPa).

The Fig. 8 represents the evolution of the pore pressure in the point B* (i.e. along the direction of the minimum stress), for the three different configurations. The evolution of the pore pressure is characterized by an initial increase, corresponding to the drilling phase. Then there is a progressive decrease of the pressure, until the steady state condition. It is interesting to observe that the path is not monotonic, resembling a behavior comparable with the so called Mandel-Cryer effect observed in the two-dimensional consolidation.

The Fig. 9 represents the evolution of the deviatoric plastic strain in the point B,

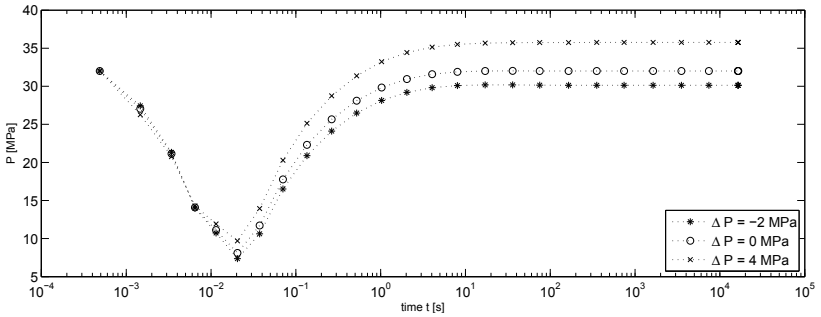

Figure 7: Pore pressure of point A* with different value of mud pressure.

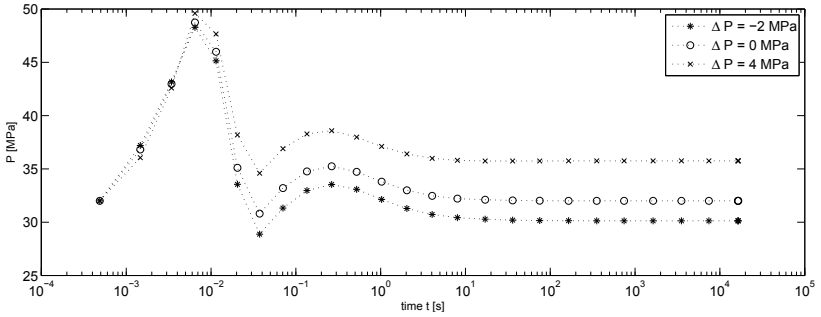

Figure 8: Pore pressure of point B* with different value of mud pressure.

extrapolated from the closest Gauss Point. The point has been selected since it is situated in the region where plastic deformations are localized. As can be observed, there is firstly an increase of plastic strain associated with the drilling process, and secondly a further increase due to the diffusion of the fluid, until the domain reaches the steady state condition. Depending on the applied mud pressure, the amount of the accumulated plastic strain changes accordingly: an increase of the mud pressure reduces the value of the plastic deviatoric strain, limiting the plastic zone. Since the plasticity is associated with the linear side of the yield surface, the evolution of the deviatoric and volumetric plastic strain are proportional, and therefore the volumetric strain follows the same path.

5 CONCLUSION

This work investigates the drilling process of a horizontal wellbore in a fully saturated rock formation, taking into account the coupling effects between the fluid and solid phases. Results of the analysis show the capability of the numerical simulations to describe the complete process. Fundamental is the detection of the plastic zones, which can be considered to assess the stability of the wellbore and the sand production.

Due to the impact that this topic has in the oil and gas industry, this subject may be extensively further developed. In particular, the analysis of different in-situ stress

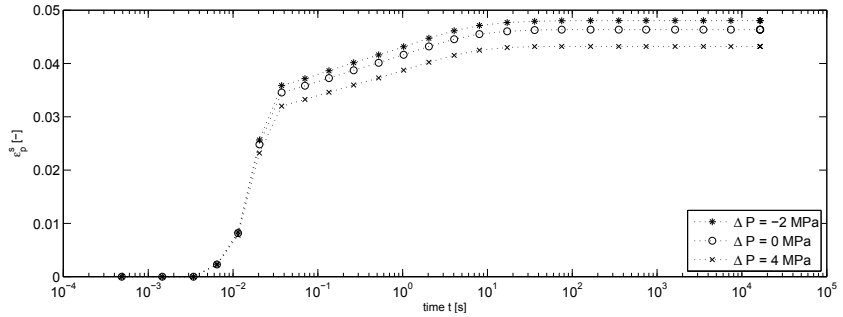

Figure 9: Deviatoric plastic strain of point B with different value of mud pressure.

and pressure configurations should be considered. The evolution of the porosity and permeability in the rock formation associated with the deformations should be assessed. Furthermore, this proposed formulation, based on finite strains assumptions, can be particularly suitable to analysis the eventual band localization around the wellbore, which can have dramatic consequences in the reservoir exploitation.

AKNOWLEDGMENTS

Financial support was provided to the first author by Gini Foundation, while part of this research was being conducted at Stanford University. Prof. R.I. Borja (Stanford University), provided the much appreciated motivation and inspirational support.

REFERENCES

[1] Moss, D., Peska, P., Finkbeiner, T., and Zoback, M., Comprehensive wellbore stability analysis using quantitative risk assessment, *Jour. Petrol. Sci. and Eng., Spec. Issue on Wellbore stability* (2003) **38**:97–109.

[2] Zoback, M. D., *Reservoir Geomechanics*, Cambridge University Press (2010).

[3] Chen, S. L., Abousleiman, Y. N. and Muraleetharan, Closed-form elastoplastic solution for wellbore problem in strain hardening/softening rock formations, *Int. J. Geomech.* (2012) **12**:494–507.

[4] Preisig M. and Prvost J.H., Fully coupled simulation of fluid injection into geomaterials with focus on nonlinear near-well behavior, *Int. J. Numer. Anal. Meth. Geomech.* (2012) **36**:1023–1040.

[5] Rutqvist, J., et al. Coupled multiphase fluid flow and wellbore stability analysis associated with gas production from oceanic hydrate-bearing sediments. *Journal of Petroleum Science and Engineering* (2012) **92**:65–81.

[6] Macinia P., Mesinia E., Salomoni V.A., Schrefler B.A., Casing influence while measuring in situ reservoir compaction, *Journal of Petroleum Science and Engineering* (2006) **50**:40–54.

[7] Song X., and Borja R.I., Mathematical framework for unsaturated flow in the finite deformation range. *International Journal for Numerical Methods in Engineering* (2014) **97**:658–682.

[8] Cuss, R. J., Rutter, E. H., and Holloway, R. F., Experimental observations of the mechanics of borehole failure in porous sandstone., *International Journal of Rock Mechanics and Mining Sciences* (2003) **40**:747–761.

[9] Simo, J.C., Algorithms for static and dynamic multiplicative plasticity that preserve the classical return mapping schemes of the infinitesimal theory, *Computer Methods in Applied Mechanics and Engineering* (1992) **99**:61–112.

[10] Carroll, M. M., A critical state plasticity theory for porous reservoir rock, *Recent Advances in Mechanics of Structured Continua* (1971) **97**:935–950.

[11] Stefanov, Y. P. and Chertov, M. A. and Aidagulov, G. R. and Myasnikov, A. V., Dynamics of inelastic deformation of porous rock and formulation of localized compaction zones studied by numerical modeling, *Journal of the Mechanics and Physics of Solids* (2011) **59**:2323–2340.

[12] Coelho, L. C., Soares, A. C, Ebecken, N. F. F., Alves, J. L. D., Lau, L., The impact of constitutive modeling of porous rocks on 2-D wellbore stability analysis *Journal of Petroleum Science and Engineering* (2005) **46**:81–100.